J. Space Weather Space Clim. 2024, **14**, 33

https://doi.org/10.1051/swsc/2024029

JSWSC

Available online at:
www.swsc-journal.org

RESEARCH ARTICLE OPEN ACCESS

Persistent high-latitude ionospheric response to solar wind forcing

Claudia Borries*, Pelin Iochem, Samira Tasnim, and Fredy Davis

German Aerospace Center (DLR), Institute for Solar-Terrestrial Physics, Kalkhorstweg 53, 17235 Neustrelitz, Germany

Received 12 December 2023 / Accepted 14 September 2024

Abstract – The solar wind continuously transfers energy into the Earth's thermosphere-ionosphere system and variations in the solar wind properties modify the state of the system. The modifications are best visible during storm conditions when the ingestion of extreme amounts of solar wind energy into the thermosphere-ionosphere system causes global changes in thermosphere as well as large deviations in the ionospheric electron density from its quiet conditions. This study shows that there exists a persistent impact of the solar wind on the high-latitude electron density. A data set of 22 years of Total Electron Content (*TEC*) and 15 years of ionosonde data (critical frequency *foF2* and height of maximum electron density *hmF2*) at Tromsø (70°N, 19°E) are used for correlation analyses with different solar wind parameters from OMNIWEB hourly "Near-Earth" solar wind magnetic field and plasma data. The results show that the ionospheric parameters systematically respond with an increase or decrease depending on local time, season, and solar cycle. *TEC* and *foF2* increase with solar wind energy during winter night conditions and decrease with increasing solar wind energy during summer daytime. The summer negative ionospheric response is more intense during high solar activity conditions, while the winter positive ionospheric response is stronger during low solar activity. An anomaly is observed around 10 UT (noon) when *TEC* and *foF2* respond with an increase during low solar activity conditions. Plasma convection, particle precipitation and Joule heating are the main drivers of the observed electron density changes at Tromsø. Local time, season, and solar cycle changes in the background ionosphere-thermosphere conditions lead to different effects of these driving processes. The results help to better understand the variability of the high-latitude electron density and show that solar wind forcing causes a systematic and persistent response of the ionosphere, which alternates depending on local time, season, and solar cycle.

Keywords: Ionosphere / Coupling / Auroral zone / Solar wind / Convection / Joule heating

1 Introduction

The state and variability of the ionosphere are relevant for many technical applications, e.g. in the communication and navigation sector, because of its impact on radiowave propagation. The ionospheric variability is strongly linked to thermospheric conditions and geomagnetic activity via complex electrodynamic coupling processes. Electromagnetic forcing from the Sun is the main driver of thermosphere-ionosphere variations, mainly through the solar EUV irradiance (e.g. Lean et al., 2011) but also through the solar wind (e.g. Lei et al., 2008a; Pedatella & Forbes, 2011). The solar wind forcing is strongest in high latitudes, where open magnetic field lines connect to the interplanetary magnetic field (Dungey, 1961; Prölss et al., 1988). The energy input from solar wind becomes most obvious during storm conditions when large amounts of energy are transferred from the solar wind into the Earth's geosystem (e.g. Tsurutani et al., 2004; Schunk & Zhu, 2008). This energy is partially stored in the magnetotail (and later released during substorms) and partially deposited in the ionosphere-thermosphere via Joule heating. The high-latitude heating processes play a crucial role in the modification of the global ionosphere-thermosphere conditions (e.g. Rodger et al., 2001; Wilson et al., 2006; Lu et al., 2016; Heelis & Maute, 2020).

A positive correlation between solar wind dynamic pressure and Joule heating has been derived in Palmroth (2004). According to their simulation, increasing dynamic pressure increases the field-aligned current (FAC) intensity, which then increases Joule heating. Also, Ritter et al. (2004) showed a correlation of solar wind with FACs, but in this case with the Kan-Lee merging electric field (Kan & Lee, 1979). A seasonal dependence of FAC strength, with the FAC intensity being much stronger in summer than in winter, can be observed (Weimer, 2001; Coxon et al., 2016; Milan et al., 2017; Workayehu et al., 2020) because the intensity of FAC depends on the conductivity in the auroral ionosphere, which is mainly modified by solar EUV irradiance and particle precipitation. Consequently, a seasonal and local time dependence also exists for Joule heating.

*Corresponding author: claudia.borries@dlr.de

In fact, Joule heating is about 50% stronger during summer than in winter (Foster et al., 1983; Fuller-Rowell et al., 1996).

Particles precipitating into the polar ionosphere partially ionise the neutral atmosphere and heat the electrons. In particular soft electron (<500 eV) precipitation, which occurs in the dayside cusp region and pre-midnight sector of the auroral zone, can cause a strong increase in the electron density and temperature in the F region. It contributes to thermosphere heating (Rentz, 2009; Zhang et al., 2012) and topside ionospheric upflows (Su et al., 1999).

Since the ionospheric response to solar wind variability is strongest during storm and substorm conditions, it has been mostly studied during these conditions. Average characteristics of the ionospheric storm evolution have been derived with statistical analyses of the F2 layer critical frequency (*foF2*, e.g. Araujo-Pradere et al., 2002; Tsagouri & Belehaki, 2008) and of Total Electron Content (*TEC*) observations (Mendillo, 2006). They show that the storm perturbations depend on a large extent on geomagnetic latitude and storm time. A classification of storms by season and local time of onset reveals a strong dependence on these parameters (Borries et al., 2015). Experiments with numerical models of the coupled thermosphere and ionosphere showed that differences between the background circulation in the summer and winter hemisphere are the explanation for the seasonal patterns in the ionospheric storm characteristics (Fuller-Rowell et al., 1996).

A long-duration solar wind impact on the thermosphere-ionosphere system has been reported for a period from 2005 to 2006, when rotating solar coronal holes caused recurrent geomagnetic activity. The resulting recurrent geomagnetic activity caused changes in electron density, TEC, neutral density, temperature, composition and winds (e.g. Lei et al., 2008a,b; Thayer et al., 2008; Crowley et al., 2008; Pedatella et al., 2010; Grandin et al., 2015). The authors attributed these thermosphere-ionosphere changes to some combination of effects due to chemical loss, neutral winds and disturbance dynamo-driven electric fields. Also, other studies show clear indications of a persistent solar impact on the ionosphere. For example, Girish et al. (1997) showed correlations of the day-to-day variability of *TEC* at high-latitude Goose Bay station and mid- latitude Sagamore Hill station with four solar wind coupling parameters, including the well-known Akasofu Epsilon parameter ε. They showed the highest (negative) correlation during winter and equinox conditions. Birch and Hargreaves (2020) found a concurrent occurrence of periodic ripples in the solar wind, the geomagnetic flux and ionosphere F-region electron density, which had about 25 min period. Cai et al. (2021) showed that high-latitude forcing can be an important source of *TEC* day-to-day variability during geomagnetically quiet conditions. However, according to our knowledge there does not yet exist a study on the persistent solar wind impact on the ionosphere.

The thermospheric behaviour at high latitudes is typically dominated by the dissipation of energy originating from the solar wind and this energy source is operating continuously, even if there is no magnetic activity (Prölss et al., 1988). Additionally, Crowley et al. (2008) stated that the processes creating neutral composition changes during geomagnetic storms occur at all activity levels. Since thermospheric heating and composition changes affect the electron density, there must be an ionospheric response to solar wind variability at all activity levels, too.

Based on the above-mentioned seasonal variation of ionospheric key parameters such as conductivity and Joule heating, we hypothesise and analyse that there is an ionospheric response to solar wind variability at all geomagnetic activity levels, which varies with local time, season, and latitude. Because the solar wind impact on the ionosphere is most immediate at high latitudes, we intend to study the seasonal dependence of the high-latitude ionospheric response to solar wind forcing. The goal of this study is to characterize the correlation between ionospheric electron density and solar wind forcing and to discuss the mechanisms causing the high-latitude ionospheric response to solar wind.

2 Data and methods

2.1 Ionospheric data

Tromsø ionosonde (TR169, geographic coordinates: 70°N, 19°E, apex coordinates on 1st Jan 2020: 67°N, 101°E) data has been available since 2005 with a temporal resolution of 15 minutes. It covers two periods of low solar activity (2005–2010 and 2016–2020) and one period of high solar activity (2011–2015). We use the F2 layer critical frequency *foF2* and the height of the maximum F2 layer electron density *hmF2*. hourly averages are calculated before generating a time series for each UT separately. This results in a 24-time series with a daily resolution of *foF2* and *hmF2*, one time series per UT. The resulting data is shown in Figure 1, second and third panel, with each line representing an individual time series. There are data gaps (indicated with grey colors), especially during the night conditions. *foF2* varies with local time (the solar local time at Tromsø is about 1.3 h past UT), season, and the solar cycle. The maximum values are observed during local daytime, summer and high solar activity intervals. Minimum values occur during local night conditions. *hmF2* decreases during low solar activity intervals, and is largest during high solar activity night conditions.

Widely used and validated global ionosphere maps are provided by the International GNSS Service (IGS). We use the 2-hour resolution *TEC* data in the time range 1998 to 2020, covering two solar cycles and extract the data at the grid point of Tromsø (70°N, 20°E). The *TEC* data is restructured into 12 individual time series with daily resolution, containing *TEC* at the different UT times. The time series are shown in image format in Figure 1, top panel. Solar cycle, (semi-)annual, and local time dependencies similar to *foF2* are clearly visible. *TEC* extracted from *TEC* maps contains spatial averages for a larger region (2.5° × 5°) and is not much affected by small-scale irregularities.

The equivalent slab thickness τ of the ionosphere represents the width or shape of vertical electron density profiles. It is defined by the ratio of the *TEC* and the peak electron density *NmF2* and thus easy to measure (Miro et al., 1999; Jakowski et al., 2017). Since it is sensitive to temperature and composition changes in the thermosphere and plasma redistribution processes, it has a high potential for exploring the dynamics of ionospheric perturbation processes. Here, we compute τ from IGS *TEC* and TR169 *foF2*, which is translated to *NmF2*. In Figure 1, the bottom panel shows the equivalent slab thickness data used for the study. The slab thickness is observed lowest

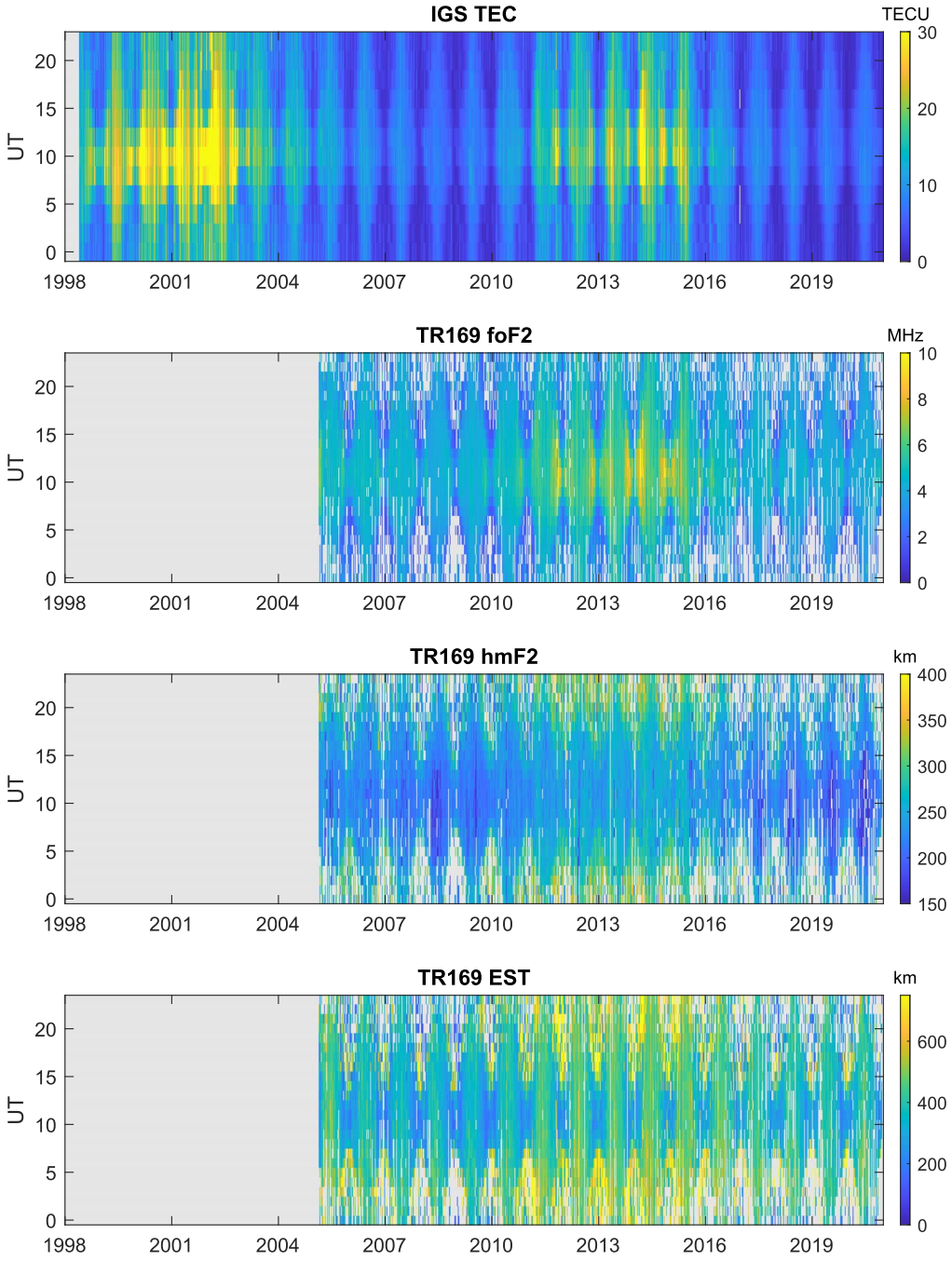

Figure 1. First Panel: IGS *TEC* data at 70°N, 20°E with 2 h temporal resolution. Second Panel: Ionosonde observation of critical frequency of the F2 layer, *foF2*, at Tromsø ionosonde TR169. Third Panel: height of F2 layer, *hmF2*, at Tromsø ionosonde TR169. Fourth Panel: Equivalent slab thickness at Tromsø ionosonde TR169. All data is gridded per UT and day (Local time is UT+1.3 h). Grey colors represent data gaps.

during winter day conditions and highest during winter night conditions, especially during high solar activity. However, since *foF2* data is very sparse during winter night conditions, we also obtain sparse data for the equivalent slab thickness during that time.

2.2 Solar wind and solar activity data

UV and EUV irradiances are the main drivers of ionization processes and thus, ionospheric electron density typically shows a high correlation with solar activity proxies. The solar radio flux at 10.7 cm (F10.7) is a widely used index of solar activity (Tapping, 2013). It describes solar UV and EUV forcing of the upper atmosphere (Floyd et al., 2005). In the auroral region investigated here, the correlation between F10.7 and *TEC* decreases due to low solar inclination angle and polar night conditions (Vaishnav et al., 2019). The Ottawa 10.7-cm radio flux adjusted to 1 AU, used in the present work, is illustrated in Figure 2. The top panel, shows the F10.7 index with a daily resolution in grey and the 2-year moving average in red.

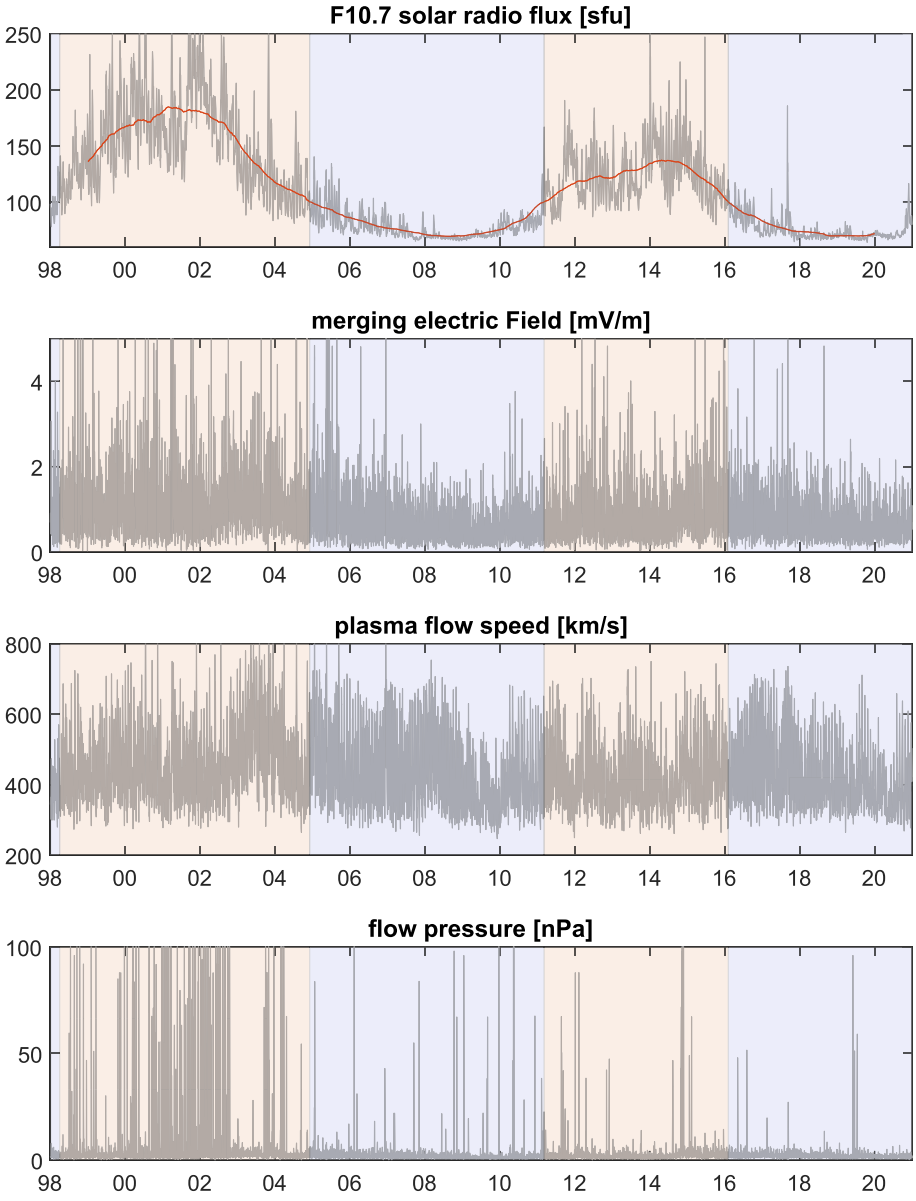

Figure 2. First panel: solar radio flux F10.7 cm index in grey and 2 years moving average in red. Second panel: Solar wind Kan-Lee merging electric field. Third panel: solar wind plasma flow speed. Bottom panel: solar wind flow pressure. All solar wind data is derived from th OMNI database. In all panels periods of solar activity maxima are indicated with red shading and solar activity minima with blue shading.

The 2-year moving average is used to identify intervals above 100 sfu, which describe high solar activity periods throughout this work. The high solar activity periods are indicated with red shading and the low solar activity periods with blue shading. In the analysis period of this work, there are two periods of high solar activity (1998–2004 and 2011–2015) and two periods of low solar activity (2005–2010 and 2016–2020).

We work with solar wind and Interplanetary Magnetic Field (IMF) observations obtained from the OMNI hourly "Near-Earth" solar wind magnetic field and plasma parameter data. The data is derived from several spacecraft in geocentric or L1 (Lagrange point) orbits, at about 1.5 million km distance from Earth. We use the IMF components B_y and B_z (in geocentric solar magnetospheric coordinates, GSM) and the plasma flow speed v to compute the Kan-Lee merging electric field as $E_{sw} = vB_t\sin^2(0.5\theta_c)$ with the transversal magnetic field $B_t = \sqrt{B_y^2 + B_z^2}$ and the clock angle $\theta_c = \arctan(B_y/B_z)$. E_{sw} is a solar wind coupling function, which can be assumed to be related to the magnetospheric convection electric field. The magnetospheric electric convection field maps down into the ionosphere, where it is driving plasma convection from the dayside to the night side across the polar cap (e.g. Lockwood et al., 1990; Milan et al., 2017; Zhang et al., 2015). We also use the OMNI solar wind flow pressure. It is an indicator of the compression of the magnetosphere and enhancement of magnetospheric currents (Palmroth, 2004).

In the rest of the paper, we refer to the plasma flow speed as solar wind speed v_{sw}. The whole dataset of solar wind parameters used in this work is illustrated in Figure 2.

The data is used with one hour temporal resolution and a moving average with a window size of 1 day is applied. This reduces, but does not eliminate the impact of storm conditions (strong perturbations in the solar wind and IMF). After the application of the moving average, the data is binned for each UT separately, such that 24-time series with a daily temporal resolution are generated (similar to the ionospheric data).

2.3 Correlation with a moving window method

The working hypothesis of this manuscript is that the ionospheric response to solar wind variability changes with season. Thus, it can be assumed that the correlation between solar wind variability and ionospheric variability is not constant. For that purpose, we are applying a cross-correlation analysis with a moving window. Because the objective is to extract seasonal effects, the correlation window is set to 90 days. A Gaussian window is used, which has the advantage to reduce the effect of values close the the edge of the window. The cross-correlation coefficient of the solar wind and ionospheric parameters is calculated for each window separately and located in time at the center of the window. The window is shifted by one day. This windowed cross-correlation analysis is performed for each UT separately. This results in a matrix of correlation coefficients containing a value for each UT and day. Data gaps reduce the number of data points used for the cross-correlation. In order to obtain statistically meaningful results, the correlation value is provided only if there are at least 60 data values of each signal in the window to correlate.

3 Results

The correlation between solar wind merging electric field E_{sw} and the ionospheric parameters at Tromsø is shown in Figure 3. The results of the correlation with *TEC* (top panel) show positive (yellow color) and negative (blue color) correlation values with magnitudes up to ±0.7. Positive correlation is most prominent during Tromsø winter (November to February) night conditions. Another positive correlation is observed during solar minimum conditions (2005–2010 and 2016–2020) at noon in a very narrow time band (10 UT). It means that during this period, *TEC* increases with E_{sw}. In general, the correlation values tend to be more positive during low solar activity conditions. A negative correlation can be observed during high solar activity conditions (1998–2004 and 2011–2015) in summer daytime (at Tromsø, summer daytime covers almost 24 h due to polar day). During these times, *TEC* decreases with increasing E_{sw}. Only during noon conditions, the correlation is around zero during high solar activity.

The results of the solar wind merging electric field correlated with *foF2* (Fig. 3, second panel) show very similar correlation values compared to *TEC*. During summer conditions, the correlation values are negative and even lower than in *TEC*. The strongest negative correlation is likewise during summer day conditions during high solar activity. Although there are many data gaps in the ionosonde data at winter night time, the positive correlation of *foF2* with the solar wind is still detectable.

The results of the solar wind merging electric field correlated with *hmF2* (Fig. 3, third panel) show a rather different picture compared to *TEC* and *foF2*. Again, there exist positive and negative correlation periods. The positive correlation occurs during winter noon conditions, indicating that at these times, *hmF2* increases with E_{sw}. Negative correlations are not as strong in magnitude as in *foF2* and *TEC*.

For the correlation of solar wind merging electric field and ionospheric equivalent slab thickness τ, an almost continuous positive correlation can be observed during noon. Thus, τ increases with E_{sw} during noon time. During high solar activity, this positive correlation can be observed throughout summer daytime condition, i.e. throughout the day. Negative correlation patterns are not very strong. When a negative correlation occurs, it occurs predominantly during winter night conditions.

To get a measure of how much solar activity impacts the ionospheric variability at the location studied here (near Tromsø), we apply the same correlation analysis with a 90-day moving window to F10.7 cm solar radio flux index. Since F10.7 index has a daily temporal resolution, each UT dependent ionosphere time series gets correlated with the same F10.7 index. The results are presented in the same way as Figure 3, the same way as it has been done for E_{sw}. The correlation coefficients reach the same magnitude as for the solar wind E_{sw}. However, they change very quickly with time and do not show as well-defined seasonal patterns as the correlation with the solar wind. As expected, Figure 4 shows generally a higher positive correlation during high solar activity periods. The correlation is weaker during the second solar maximum period, which is attributed to the fact that the second solar maximum was weaker than the first.

To show the seasonal dependence of the correlation results, an average of the correlation values is estimated for each day of the year and UT. In that case, we do not distinguish the solar cycle effects. The average correlation estimates illustrated in Figure 5 are computed using a minimum variance unbiased estimator (Alexander, 1990). We add to the results of E_{sw} (first row) and F10.7 (last row) the average correlations for the solar wind dynamic pressure p_{sw} (second row) and solar wind speed v_{sw} (third row). To allow the identification of day and night conditions, sunrise and sunset times at 250 km altitude are indicated with yellow lines.

For all the solar wind parameters, the correlation with *TEC* (first column) and *foF2* (second column) show similar characteristics. The correlation coefficients are positive in winter night conditions and negative in summer day conditions (except noon). The strongest positive correlation can be observed for the correlation between E_{sw} and *TEC*. The strongest negative correlation can be observed for the correlation between v_{sw} and *foF2*. The correlation of solar wind parameters with the equivalent slab thickness τ (third column) is mostly positive with the highest correlation during noon time. *hmF2* (last column) shows a clear positive correlation with E_{sw} and v_{sw} only during winter noon conditions. p_{sw} shows the weakest correlation among all solar wind parameters.

In the correlation with the F10.7 index (last row), *TEC* shows the highest values, especially during summer day conditions. The average correlation of the F10.7 index with *foF2*, *hmF2*, and τ is very weak. Overall, the magnitude of the average correlation of the ionospheric parameters with the F10.7 index is much smaller than for E_{sw} and v_{sw}.

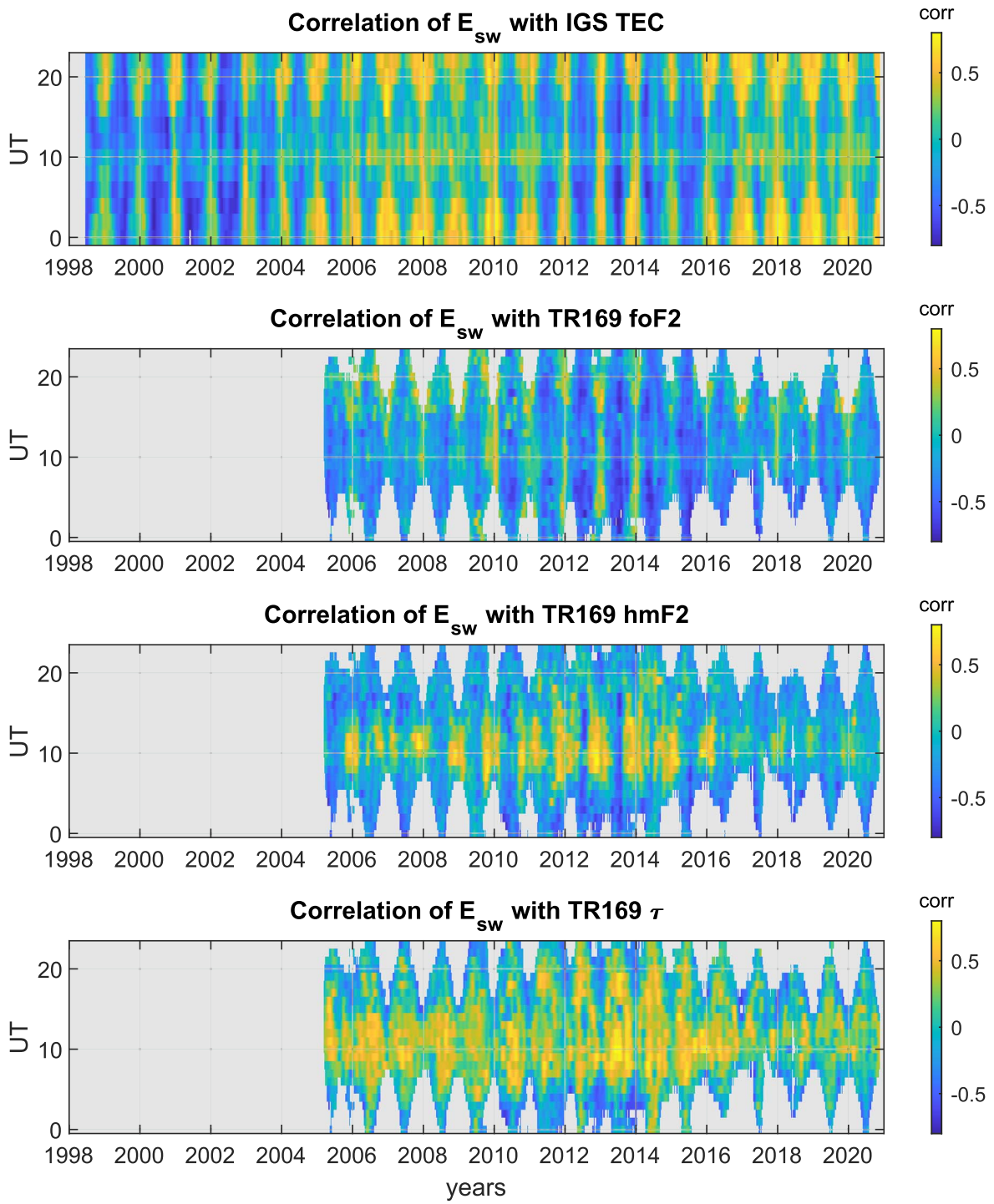

Figure 3. Correlation of the ionospheric parameters *TEC*, *foF2*, *hmF2*, and τ at Tromsø with the solar wind merging electric field. Missing data is indicated in gray shading.

In Figure 5, all correlation results between ionospheric F2-region parameters and solar wind parameters show an anomaly during noon-time, when the correlation coefficients are typically larger than before and after. A more detailed look into Figure 3 shows that during summer conditions, the correlation coefficients of *TEC* and E_{sw} at 10 UT are always about a value of 0.5 larger than at 5 UT and 15 UT.

4 Discussion

4.1 Joint impact of solar activity and solar wind

The ionospheric variability at Tromsø depends on both, solar activity and solar wind variability. This is reflected in the results with the observation that both F10.7 index and E_{sw} show similar magnitudes of the correlation coefficients obtained

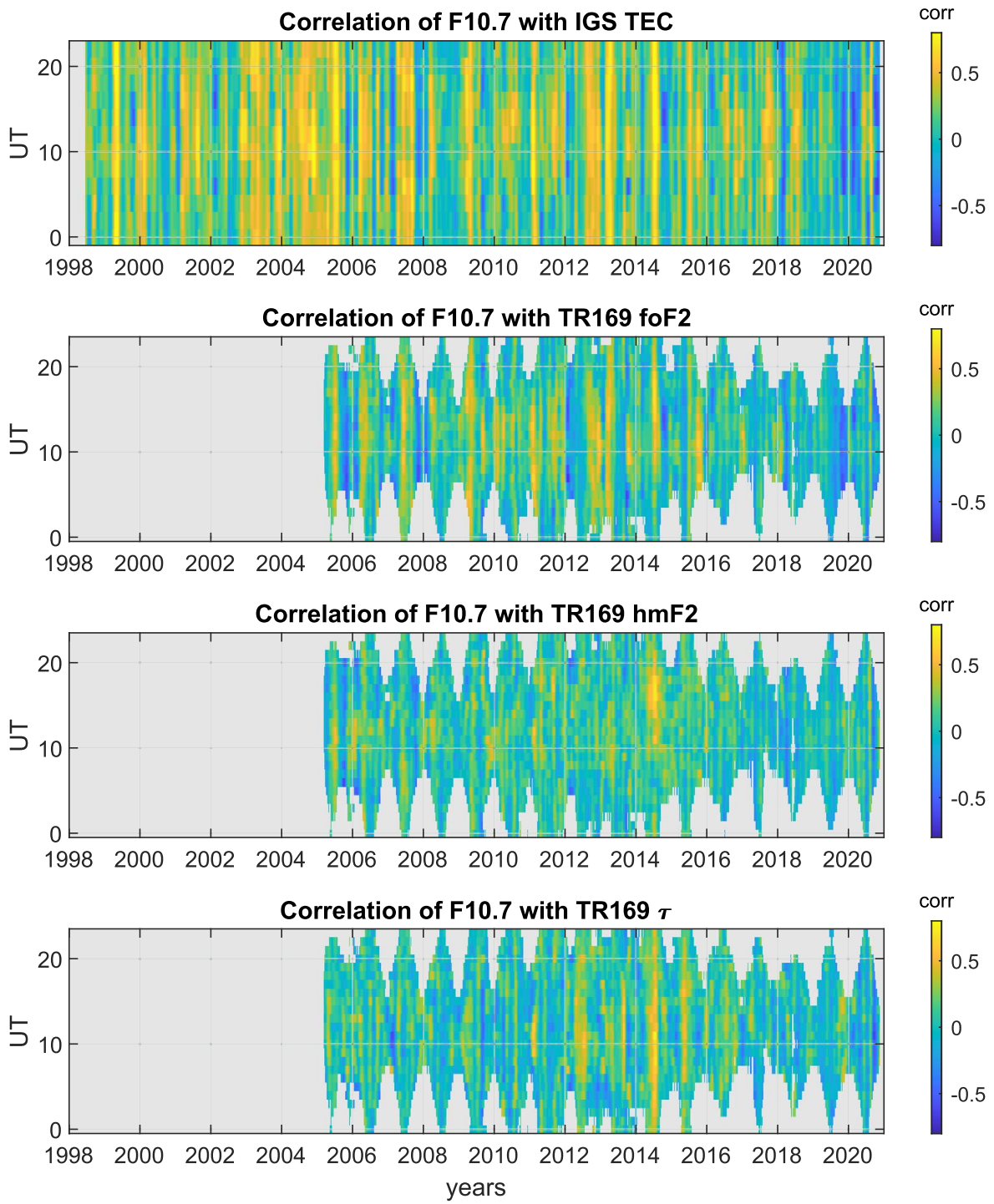

Figure 4. Correlation of the ionospheric parameters *TEC*, *foF2*, *hmF2*, and τ at Tromsø with the solar activity index F10.7. Missing data is indicated in gray shading.

in a 90-day moving window. Although the expectation would be to get only positive correlation coefficients for the correlation between F10.7 and the ionospheric parameters *TEC* and *foF2*, the actual correlation coefficients fluctuate between positive and negative values. In a time window of 90 days, the main period of the F10.7 solar radio flux index is the solar rotation period, which is 27 days. The solar rotation period is also a strong spectral component in the solar wind variability. Thus, negative correlation coefficients between F10.7 and *TEC* at Tromsø will reflect a response to solar wind variability and not a response to solar EUV irradiance. It needs to be taken into account that the solar zenith angle, which is even more important to the ionization than solar EUV irradiance variability, changes a lot at Tromsø during the 90-day window, which is

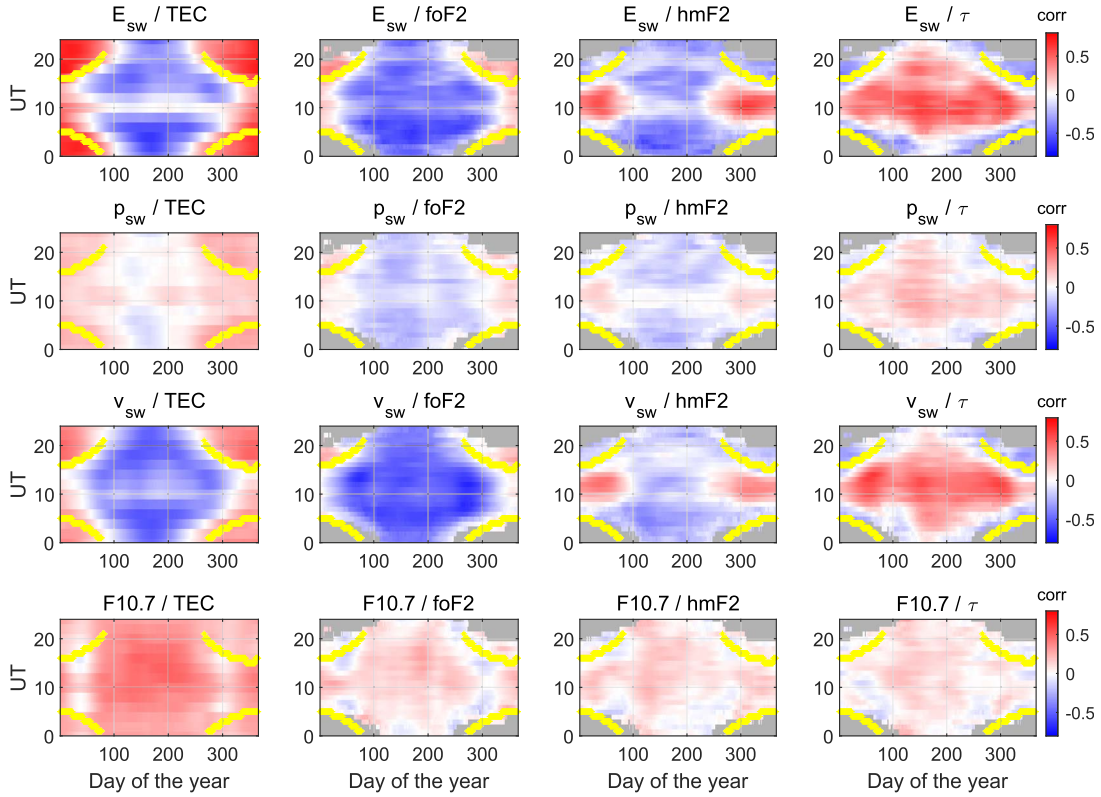

Figure 5. Average cross-correlation per day of the year and UT between ionospheric parameters at Tromsø with the merging electric field (top row), the solar wind dynamic pressure (second row), the solar wind speed (third row) and the solar activity index F10.7 (last row). Sunrise and sunset at an altitude of 250 km are indicated with a bold yellow line. Missing data is indicated in gray shading.

yet another factor that reduces the correlation between F10.7 and ionospheric parameters. The fact that solar EUV irradiance and solar wind impact the ionospheric parameters at the same time explains that the magnitude of the correlation coefficients in all results seldom exceeds ≈0.8. However, the regular local time and seasonal changes in the correlation between ionospheric and solar wind parameters indicate a persistent solar wind impact on the ionosphere at Tromsø.

4.2 Coupling processes during winter conditions

During winter (December–February), there is night condition at Tromsø most of the time (polar night). A positive correlation is observed between solar wind parameters E_{sw}, v_{sw}, and p_{sw} with *foF2* and *TEC*. It describes an increase in *TEC* with solar wind forcing. This result agrees with the statistical storm study presented by Borries et al. (2015), which revealed that very strong *TEC* enhancements occur in high latitudes during nighttime and only during the winter season. These *TEC* enhancements were well correlated with solar wind energy input, which has been represented in this study by IMF B_z and a variant of E_{sw}. The results presented here show the highest positive correlation for E_{sw}. Thus, it can be assumed that plasma convection driven by the solar wind coupling is an important process modifying the ionosphere electron density. Also, plasma resulting from soft particle precipitation in the auroral oval can be involved in the convection process (Lockwood et al., 1984). This leads to an increase in the nightside high-latitude ionospheric electron density in the F-region. The magnetic field lines at Tromsø have an inclination of 77° (c.f. Ogawa et al., 2010). Anti-sunward $E \times B$ plasma drifts, as initiated by the convection electric field under conditions of negative B_z component of the interplanetary magnetic field, will have an upward component on the dayside and a downward component on the nightside (c.f. schematic illustration in Fig. 6). This will lead to a rise of *hmF2* during day and decent during night with increasing solar wind energy. In good agreement, *hmF2* shows a positive correlation with the merging electric field during winter day conditions. This is a strong indication that high-latitude electron density changes during winter are strongly driven by magnetospheric electric convection field resulting in anti-sunward plasma convection across the polar cap. Precipitation of energetic particles from the magnetotail is certainly another factor that increases the electron density during winter night conditions. Seasonal effects on auroral particle precipitation have been described in e.g., Liou et al. (2001). Nightside (≈1900–0300 MLT) auroral power is suppressed in summer and the average energy of precipitating electrons is higher in the dark than in the sunlit hemisphere. More than half of the energy deposited by precipitating auroral electrons goes into heating the neutral atmosphere (Brekke, 1982; Rees et al., 1983). There are long-time constants associated with some processes that contribute to heating so that there is a time lag between energy deposition and heating (Rees et al. 1983). Thus, it can be that auroral particle precipitation first increases the electron density by ionization and a few hours later composition changes due to heating increase the recombination

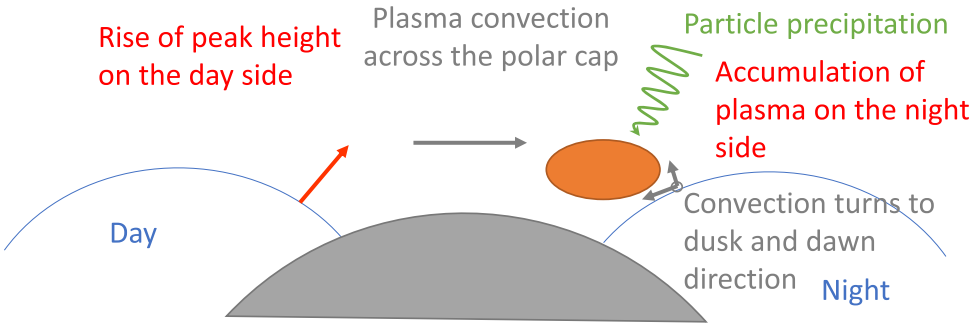

Figure 6. Schematic illustration of anti-sunward plasma convection as main driver for the observed correlation pattern between solar wind and ionospheric parameters.

rate leading to a decrease in the electron density. Further analyses of ionospheric response times are planned in a follow-up study to investigate and separate different processes leading to the ionospheric response to solar wind variability in high latitudes.

The cross-polar cap ion convection usually stimulates ion-driven neutral winds due to collisions, which can become intense during storm conditions (Killeen et al., 1995). The Tromsø location is affected by these ion-driven winds, as shown by Oyama et al. (2023). The authors provide a statistical analysis of thermospheric winds measured with the Fabry-Perot Interferometer at Tromsø, and the results show well, how the ion-driven winds enhance with increasing geomagnetic activity.

The careful reader may have noticed that the results of Girish et al. (1997) showed a negative correlation of solar wind parameters with *TEC* at the sub-auroral station Goose Bay. This station is located outside the auroral oval (magnetic latitude 59°N) and thus it is not affected by the plasma convection and the particle precipitation as it occurs in the auroral oval. Hence, the winter night-time enhancement of *TEC* with solar wind energy does not occur at sub-auroral latitudes.

4.3 Coupling processes during summer conditions

During summer, Tromsø has polar day conditions and is thus sunlit most of the time. The correlation coefficients of the solar wind parameters with *TEC*, *foF2*, and *hmF2* are mainly negative with the peak coefficients at about 5 UT. The correlation with τ, which is mainly positive during noon, indicates an increase of neutral temperature with solar wind energy input. During noon, the average correlation coefficients are larger than during morning and afternoon hours for all parameters. To better illustrate these correlation characteristics during summer, the correlation coefficients for the July 1st of each year are shown in Figure 7. The average correlation results are shown for three solar wind coupling functions (Fig. 5), the Kan-Lee merging electric field E_{sw}, the solar wind dynamic pressure p_{sw} and solar wind speed v_{sw}. The strongest correlation during summer is obtained from the correlation of the solar wind speed v_{sw} with *foF2*. The solar wind speed is an important parameter, driving the magnetospheric electric convection field. It contributes to the increase in plasma transport. It is worth mentioning that the correlation between solar wind speed and ionospheric parameters during summer time is negative throughout the solar cycle (not shown here), while the correlation with merging electric fields tends towards zero during low solar activity summer conditions (c.f. Fig. 3). Further analysis is needed to better understand the coupling processes that lead to this observation. The solar wind dynamic pressure has been discussed in e.g., Palmroth (2004) to cause a compression of the magnetosphere, an increase in magnetosphere currents, and finally an increase in Joule heating. Since the correlation between p_{sw} and ionospheric parameters is weakest among all solar wind parameters, magnetosphere compression is not likely to be the major source of the ionospheric changes during summer. It can be argued that Joule heating increases mostly because of enhanced ion convection, which produces a larger relative flow between ions and neutrals.

The role of Joule heating is also indicated by the different summer correlation values during high and low solar activity periods (c.f. Fig. 7). The summer correlation coefficients of *TEC* are strongly negative during high solar activity (red lines), while they tend towards zero during low solar activity conditions (blue lines). Also, the summer negative correlation values of *foF2* tend to be stronger during years of high solar activity. This can be explained on the one hand by the background ionisation and thus ionospheric conductance. The conductivity in the E-region is most relevant for the Joule heating. Tromsø ionosonde *foE* observation (not shown here) which is proportional to the E-region electron density, increases with solar zenith angle and with solar activity. This variability impacts Joule heating and can explain partially the larger negative correlation coefficients during daytime and high solar activity periods. On the other hand, also the location of the auroral oval and heating regions needs to be taken into account. Most of the time, Tromsø location is within the auroral oval and heating region. Statistical studies of Joule heating show that the main heating effects take place at 2–5 and 15–18 magnetic local time at Tromsø (Cai et al., 2014). Given that thermosphere changes due to Joule heating causes a decrease in *TEC* and *foF2*, the Joule heating maxima agree well with the most negative correlation coefficients. During noon conditions, Tromsø is typically outside the heating region and the time span when Tromsø is outside the auroral oval becomes larger with decreasing geomagnetic activity (Prölss et al., 1988; Tesfaw et al., 2023). When the geomagnetic activity is lowest, Tromsø is outside the oval from 6 to 21 magnetic local time. This is another explanation showing why there is not a strong negative correlation during noon and during low solar activity conditions.

The seasonal variation of Joule heating effects has been analysed with a coupled thermosphere-ionosphere model in

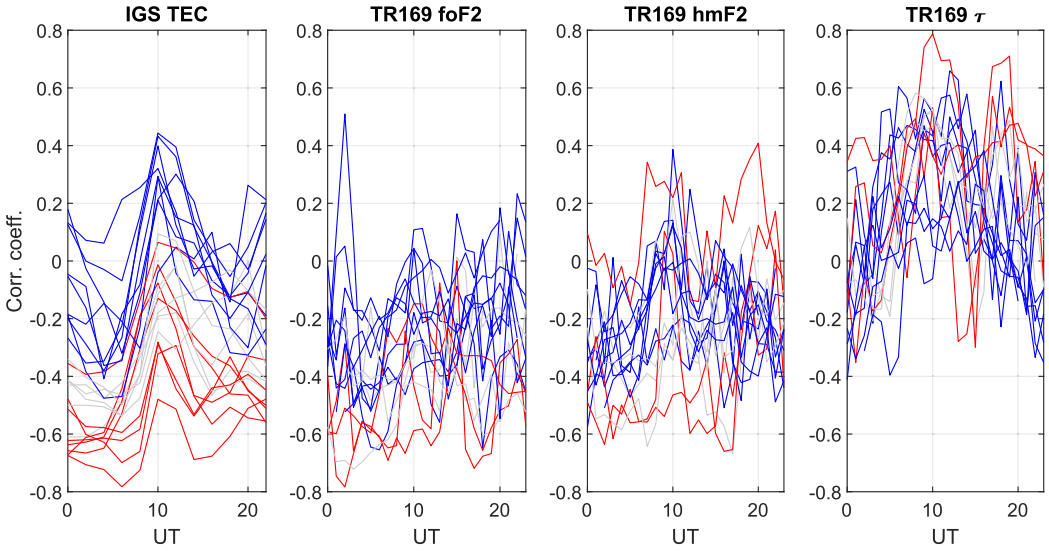

Figure 7. Correlation coefficients at 1st July each year (1998–2020) between Em_{sw} and *TEC* (first panel), *foF2* (second panel), *hmF2* (third panel), and equivalent slab thickness (last panel). Correlation coefficients at high solar activity (one-year moving average of F10.7 > 120 sfu) are red, low solar activity (one-year moving average of F10.7 < 80 sfu) are blue and other correlation coefficients are grey.

Fuller-Rowell et al. (1996). They show a high-latitude enhancement of molecular mass in response to solar wind forcing, which is stronger during summer conditions than in winter. This hemispheric difference is found to be caused by larger conductivity in summer and 50% stronger Joule heating. The heating causes an upwelling and a decrease in $[O/N_2]$-ratio. Consequently, the recombination rate becomes higher with increased solar wind impact and causes a decrease in *TEC* and *foF2*. The change in composition is considered the main driver of the negative correlation between *TEC* and *foF2* with solar wind variability. The concurrent positive correlation of τ during daytime supports this argument because it indicates an increase in temperature (Jakowski et al., 2017), preferentially caused by the Joule heating. The correlation of *hmF2* with the solar wind parameters is not as strong as for the other ionospheric parameters. It shows a negative correlation with the solar wind, which is difficult to explain without using physics-based modeling.

Grandin et al. (2015) performed a simple model study to identify the cause of the decrease of *foF2* during high-speed solar wind streams. They conclude that an increase of both ion and neutral temperature plays an important role. These temperature increases are caused by ion-neutral friction. The ion temperature increases the recombination coefficient. The neutral temperature drives the recombination by an increase of the number of molecular species caused by upwelling. These processes intensify during storm conditions and EISCAT Incoherent Scatter Radar observations of storm conditions during summer and equinox daytime at Tromsø can be used to illustrate the effect. An example is shown in Figure 8 where the EISCAT electron density distribution on 15 May 1997 and its deviation from quiet conditions is shown during a major geomagnetic storm at the beginning of the solar cycle 23. A clear electron density depletion in the F2 region is visible, which has been attributed to increased recombination caused by a strong electric field (Liu et al., 2000). Also, Ellahouny et al. (2024) observe a decrease in the electron density in EISCAT Tromsø and Svalbard radar latitude scans, which they attribute to composition changes due to ion-neutral frictional heating transported by neutral winds. Based on satellite in-situ observations different studies (e.g. Prölss et al., 1988; Liu et al., 2012) showed that the thermospheric density increases globally with solar wind impact. The density changes are strongest during summer daytime conditions. Also, a change in the $[O/N_2]$-ratio, which is inversely related to the recombination rate, is observed. The composition change differs with latitude. At high latitudes, $[O/N_2]$-ratio decreases during day and night conditions as well. The percentage difference is stronger during summer than in winter. Both density and composition changes reflect the effect of thermospheric expansion and they cause a decrease in electron density, especially during summer daytime conditions.

Decreasing $[O/N_2]$ during weak external forcing which led to a decrease in *TEC* at high-latitudes has been reported in Cai et al. (2021). The authors studied a small amount of geomagnetically quiet days and considered that the number of "quiet" days that may be influenced by low levels of geomagnetic activity is small. Our statistical study reveals that this is not the case. According to our results, there is a persistent indirect impact of solar wind on ionospheric variability, which relates partially to the solar wind energy deposition in the thermosphere. Because the dissipation of solar wind energy in the thermosphere is nearly exclusively monitored by geomagnetic indices it is also interpreted as "geomagnetic activity effect" (Prölss et al., 1988; Juusola et al., 2009).

4.4 TEC response to solar wind variability at the magnetic conjugate point

Since Prölss et al. (1988) described that solar wind-driven thermospheric disturbances depend on both solar local time and geomagnetic latitude, it can be expected that the same local time and seasonal effects discussed before for Tromsø occur similarly at its magnetic conjugate point, with some deviations due to hemispheric asymmetries (Laundal et al., 2016). This is

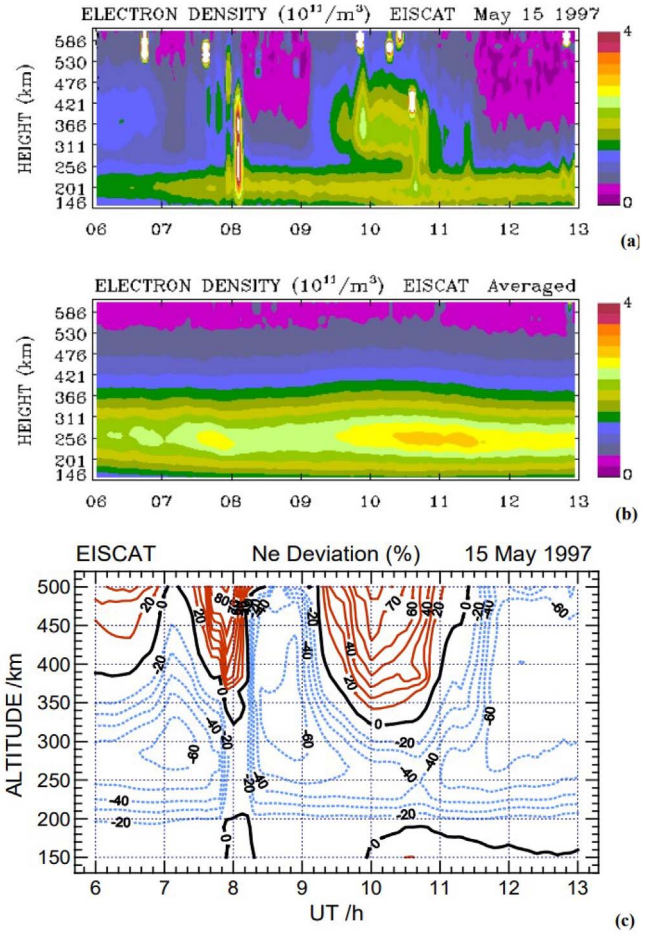

Figure 8. EISCAT observations at Tromsø: (a) Two-dimensional image of electron density distribution vs. UT and height on 15 May 1997, (b) an average of electron density distributions on some quiet days in April and June of 1997 as a reference, (c) deviation of electron density during the magnetic storm of 15 May 1997 with respect to the quiet reference (Figure from Ma et al., 2002).

confirmed by the results presented in Figure 9, which shows the correlation coefficients between *TEC* and E_{sw} at the magnetic conjugate point of Tromsø. *TEC* has been extracted from the IGS *TEC* maps at the closest grid point of the magnetic conjugate point, which has been calculated for each time step individually. The magnetic conjugate point fluctuates around −61.6±0.5° S and 63.8±1°E geographic coordinates. The correlation results at the magnetic conjugate point of Tromsø show almost the same magnitude and variation in the correlation coefficients compared to Tromsø. There is a positive correlation during winter (May-August) night conditions and a negative correlation during summer (November-February) day conditions. Also, the magnetic conjugate point shows the same solar cycle dependence as observed at Tromsø with a much stronger negative correlation during summer (December-February) when the solar activity is high. The slight difference can be explained on the one hand with sparse *TEC* observations around the conjugate point and on the other hand with hemispheric asymmetries. The consistency between the correlation results of *TEC* with E_{sw} at Tromsø and its magnetic conjugate point confirms the local time, seasonal, and solar cycle dependence of the *TEC* response to solar wind variability.

4.5 Noon-time correlation anomaly

The correlation results show an anomaly during noon-time (≈10 UT) when the correlation coefficients are larger than in the morning and afternoon hours. During high solar activity conditions, morning and afternoon are negatively correlated and at noon the correlation tends towards zero. During the low solar activity, morning and afternoon are weakly correlated and noon shows a positive correlation. This anomaly is best visible in *TEC*. The same anomaly is visible at the magnetic conjugate point of Tromsø.

As explained above (c.f. Sect. 4.3), this is partially attributed to periods when Tromsø is outside the heating region. However, especially during low solar activity conditions, the correlation between *TEC* and E_{sw} becomes positive from time to time. Thus, there must be a plasma source. An increase of *foF2* during noon time at Sodankylä ionosonde (geomagnetic latitude 64°N) in response to high-speed solar wind streams during low solar activity has been reported in Grandin et al. (2015). During the low solar activity, Tromsø and Sodankylä are typically outside the auroral oval during daytime (Tesfaw et al., 2023) and thus, subauroral effects are likely to cause the increase of *foF2*. Grandin et al. (2015) explain the increase with an enhancement of dayside auroral transients caused by increased solar wind dynamic pressure and the resulting compression of the dayside magnetosphere. So-called "midday subauroral patches" (Liou et al., 2002) and "subauroral proton flashes" (Hubert et al., 2003) can be associated with the observed noon-time increases of *foF2* and *TEC* with increasing solar wind energy. The duration of the shock-induced auroral precipitation is short (≈10 min), the enhanced plasma density they produce in the F region decays slowly and may be detected during an hour or longer (Grandin et al., 2015).

The above presented EISCAT campaign during the major geomagnetic storm on 15 May 1997 (Fig. 8) shows a noon-time increase in electron density. It has been described by (Ma et al., 2002) as a stable layer of ionization enhancement which peaked at about 350 km height during 09:10–11:30 UT. The comparison with satellite based UV data and energetic particle snapshots revealed that EISCAT was located under the polar cusp region which was highly active, and expanded greatly equatorwards due to magnetopause reconnection during long-lasting southward IMF. Simultaneously, soft particles of the magnetosheath precipitated into the F-region ionosphere and caused the electron density increase over EISCAT. This event has been associated with strong dayside aurora extending to as low as 62° N magnetic latitude (Ma et al., 2002). Based on an assessment of several months of Polar UV imager data, Liou et al. (2001) described the enhancement of dayside aurora in summer as a seasonal effect.

Another example of a short period noon-time electron density increase has been discussed in Jakowski et al. (1992) for the onset phase of a geomagnetic storm on 28–29 July, 1987, at the beginning of solar cycle 22. Using observations of the Tromsø Incoherent Scatter Radar, they showed a clear increase of the electron density with respect to quiet conditions in the F2-region at 323 km altitude. This increased electron density persisted in the period from about 9–15 UT. In this case, the authors

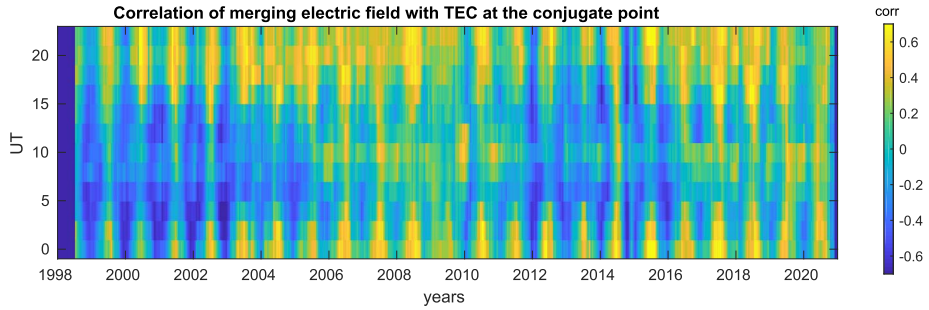

Figure 9. Correlation of the *TEC* extracted from IGS maps at the magnetic conjugate point of Tromsø with the solar wind merging electric field.

attribute the electron density increase to a rapid uplifting of plasma by $E \times B$ drift, because effects of a prompt penetration electric field have been observed globally. Poleward convection of mid-latitude plasma, which is familiar from the effects of the storm enhanced density plume and tongue of ionization (Foster et al., 2005), may have contributed to this F2-region electron density increase at Tromsø.

Hence, the noon-time anomaly in the correlation may be caused on the one hand by a decrease in Joule heating and on the other hand by additional plasma supply which can have different sources: 1) during low solar activity dayside auroral transients (precipitation from the plasma sheet) or 2) from poleward convection of mid-latitude plasma due to $E \times B$-drift or 3) during high geomagnetic activity from soft particle precipitation associated to an expansion of the cusp during strong solar wind energy input.

4.6 Delay of the ionospheric response

The ionospheric response to the solar wind is not instantaneous, as shown by Shirochkov et al. (1990). They studied the effects with minutes resolution and found a delayed response of about 40 min in the upper ionosphere. Also, Burke et al. (2007) found a delay of 4–6 h of the thermospheric density response to the electric field in the inner magnetosphere. Depending on the data filtering applied, even longer delays of the ionosphere to solar wind variability have been detected. For example, Jakowski et al. (1998) reported a negative correlation between *TEC* and solar wind speed during winter conditions with a time lag of 2–5 days and associated it with a negative storm response. The authors applied a 6-day moving average on the data before correlation, which is expected to average out the immediate positive response, which is visible in the results presented here. Further investigations are planned in a follow-up study to assess the delayed response of the ionosphere to solar wind forcing in more detail.

5 Summary and conclusions

Analysing two decades of ionospheric F2-region observations (*TEC*, *foF2*, *hmF2*, and equivalent slab thickness) at Tromsø and solar wind observations from OMNI with a cross-correlation method revealed that the solar wind energy input into the Earth system persistently causes a response of the high latitude electron density to the solar wind variability. The change in electron density alters between increase and decrease depending on local time, season and solar activity. The electron density increases with the Kan-Lee merging electric field during winter night conditions and decreases during enhancement of it in summer. Since the negative correlation between the different solar wind parameters and the ionospheric parameters *TEC* and *foF2* in summer is strongest for the solar wind speed, we conclude that the major driving process of the ionospheric response to solar wind variability is the intensification of the magnetosphere convection electric field, which maps down into the polar ionosphere and drives strong plasma convection across the polar cap.

One factor causing the systematic local time, seasonal, and solar cycle variations of the correlation coefficients is assumed to be the ionospheric conductivity, which changes mainly with the E-region electron density. Another important factor is the location of Tromsø with respect to the auroral oval. The fact that during daytime UT hours, Tromsø is most of the time inside the auroral oval during high solar activity and mostly outside during low solar activity conditions introduces a solar cycle effect in the correlation, too.

The decrease in *TEC* and *foF2* with solar wind energy input during summer, which is expected to be caused by frictional heating, is strongest in the morning hours (≈5 UT) and has a second peak in the afternoon hours. An anomaly in the correlation is present at noon-time (≈10 UT) with larger correlation coefficients than in the morning and afternoon hours. The source of this anomaly is expected to be reduced or missing heating during noon conditions and depending on the geomagnetic activity level, sub-auroral precipitation effects, plasma transport, and soft particle precipitation.

The correlation results between *TEC* at Tromsø's magnetic conjugate point and the solar wind parameters confirm the observations of the ionosphere response to solar wind variability and show that it occurs similarly at both hemispheres at the same geomagnetic latitude.

The knowledge gained about the persistent and systematic ionospheric response to solar wind forcing helps understanding the ionospheric variability at high latitudes and shows the need to include solar wind metrics in empirical ionosphere models. The detected electron density perturbations caused by the solar wind energy input agree well with the common knowledge about the processes and seasonal dependence of ionospheric storms. Studying the persistent ionospheric response to solar wind more in-depth is expected to improve the understanding of ionospheric storms in general.

Acknowledgements

We acknowledge NASA Goddard Space Flight Center for providing hourly "Near-Earth" solar wind magnetic field and plasma data via OMNIWEB (https://omniweb.gsfc.nasa.gov/ow.html), the University Tromsø and the GIRO database (http://giro.uml.edu/didbase/scaled.php) for providing the TR169 ionosonde data and the International GNSS Service (IGS) for providing *TEC* maps (downloaded from https://cdaweb.gsfc.nasa.gov) used here. The Ottawa 10.7-cm radio flux adjusted to 1 AU has been obtained from geomagnetic and solar indices collection files at ftp://ftp.gfz-potsdam.de/pub/home/obs/Kp_ap_Ap_SN_F107. We are also very grateful to S. Buchert, S.-i. Oyama, and H. Sato for fruitful discussions. The editor thanks Jaroslav Urbar and an anonymous reviewer for their assistance in evaluating this paper.

References

Alexander RA. 1990. A note on averaging correlations. *Bull Psychon Soc* **28(4)**: 335–336. https://doi.org/10.3758/bf03334037.

Araujo-Pradere EA, Fuller-Rowell TJ, Codrescu MV. 2002. STORM: An empirical storm-time ionospheric correction model 1. Model description. *Radio Sci.* **37(5)**: 1070. https://doi.org/10.1029/2001RS002467.

Birch MJ, Hargreaves JK. 2020. Quasi-periodic ripples in high latitude electron content, the geomagnetic field, and the solar wind. *Sci Rep* **10(1)**: 1313. https://doi.org/10.1038/s41598-019-57201-4.

Borries C, Berdermann J, Jakowski N, Wilken V. 2015. Ionospheric storms – A challenge for empirical forecast of the total electron content. *J Geophys Res Space Phys* **120(4)**: 3175–3186. https://doi.org/10.1002/2015JA020988.

Brekke A. 1982. Joule heating and particle precipitation. *Adv Space Res* **2(10)**: 45–53. Proceedings of the Topical Meeting of the COSPAR Interdisciplinary Scientific Commission C of the COSPAR Twenty-fourth Plenary Meeting, https://doi.org/10.1016/0273-1177(82)90362-3.

Burke WJ, Gentile LC, Huang CY. 2007. Penetration electric fields driving main phase *Dst*. *J Geophys Res Space Phys* **112(A7)**: A07208. https://doi.org/10.1029/2006ja012137.

Cai L, Aikio AT, Nygrén T. 2014. Solar wind effect on Joule heating in the high-latitude ionosphere. *J Geophys Res Space Phys* **119(12)**: 10440–10455. https://doi.org/10.1002/2014ja020269.

Cai X, Burns AG, Wang W, Qian L, Pedatella N, et al. 2021. Variations in thermosphere composition and ionosphere total electron content under "geomagnetically quiet" conditions at solar-minimum. *Geophys Res Lett* **48(11)**: e2021GL093300. https://doi.org/10.1029/2021gl093300.

Coxon JC, Milan SE, Carter JA, Clausen LBN, Anderson BJ, Korth H. 2016. Seasonal and diurnal variations in AMPERE observations of the Birkeland currents compared to modeled results. *J Geophys Res Space Phys* **121(5)**: 4027–4040. https://doi.org/10.1002/2015ja022050.

Crowley G, Reynolds A, Thayer JP, Lei J, Paxton LJ, Christensen AB, Zhang Y, Meier RR, Strickland DJ. 2008. Periodic modulations in thermospheric composition by solar wind high speed streams. *Geophys Res Lett* **35(21)**: L21106. https://doi.org/10.1029/2008gl035745.

Dungey JW. 1961. Interplanetary magnetic field and the auroral zones. *Phys Rev Lett* **6(2)**: 47–48. https://doi.org/10.1103/physrevlett.6.47.

Ellahouny NM, Aikio AT, Vanhamäki H, Virtanen II, Cai L, , et al. 2024. EISCAT observations of depleted high-latitude F-region during an HSS/SIR-driven magnetic storm. *J Geophys Res Space Phys* **129**, e2024JA032910. https://doi.org/10.1029/2024JA032910.

Floyd L, Newmark J, Cook J, Herring L, McMullin D. 2005. Solar EUV and UV spectral irradiances and solar indices. *J Atmos Sol Terr Phys* **67(1–2)**: 3–15. https://doi.org/10.1016/j.jastp.2004.07.013.

Foster JC, Coster AJ, Erickson PJ, Holt JM, Lind FD, et al. 2005. Multiradar observations of the polar tongue of ionization. *J Geophys Res Space Phys* **110(A9)**: A09S31. https://doi.org/10.1029/2004JA010928.

Foster JC, St.-Maurice J-P, Abreu VJ. 1983. Joule heating at high latitudes. *J Geophys Res Space Phys* **88(A6)**: 4885–4897. https://doi.org/10.1029/ja088ia06p04885.

Fuller-Rowell TJ, Codrescu MV, Rishbeth H, Moffett RJ, Quegan S. 1996. On the seasonal response of the thermosphere and ionosphere to geomagnetic storms. *J Geophys Res Space Phys* **101(A2)**: 2343–2353. https://doi.org/10.1029/95JA01614.

Girish T, Jayachandran B, Shamsudeen S. 1997. Influence of solar wind on the TEC variations at mid and sub-auroral latitudes during sunspot maximum. *Acta Geod Geoph Hung* **32**: 287–292. https://doi.org/10.1007/BF03325499.

Grandin M, Aikio AT, Kozlovsky A, Ulich T, Raita T. 2015. Effects of solar wind high-speed streams on the high-latitude ionosphere: superposed epoch study. *J Geophys Res Space Phys* **120(12)**: 10669–10687. https://doi.org/10.1002/2015ja021785.

Heelis RA, Maute A. 2020. Challenges to understanding the earth's ionosphere and thermosphere. *J Geophys Res Space Phys* **125(7)**: e2019JA027497. https://doi.org/10.1029/2019ja027497.

Hubert B, Gérard JC, Fuselier SA, Mende SB. 2003. Observation of dayside subauroral proton flashes with the IMAGE-FUV imagers. *Geophys Res Lett* **30(3)**: 1145. https://doi.org/10.1029/2002gl016464.

Jakowski N, Hocke K, Schlüter S, Heise S. 1998. Space weather effects detected by GPS based TEC monitoring. In: *Workshop on Space Weather, Noordwijk, 11–13 November*, vol. **ESA WPP-155**, ESTEC (Ed.), ESA ESTEC, Noordwijk, pp. 241–244. Available at https://swe.ssa.esa.int/TECEES/spweather/workshops/proceedings_w1/POSTER1/jakowski1.pdf.

Jakowski N, Hoque MM, Mielich J, Hall C. 2017. Equivalent slab thickness of the ionosphere over Europe as an indicator of long-term temperature changes in the thermosphere. *J Atmos Sol Terr Phys* **163**: 91–102. https://doi.org/10.1016/j.jastp.2017.04.008.

Jakowski N, Jungstand A, Schlegel K, Kohl H, Rinnert K. 1992. The ionospheric response to perturbation electric fields during the onset phase of geomagnetic storms. *Can J Phys* **70(7)**: 575–581. https://doi.org/10.1139/p92-093.

Juusola L, Kauristie K, Amm O, Ritter P. 2009. Statistical dependence of auroral ionospheric currents on solar wind and geomagnetic parameters from 5 years of CHAMP satellite data. *Ann Geophys* **27(3)**: 1005–1017. https://doi.org/10.5194/angeo-27-1005-2009.

Kan JR, Lee LC. 1979. Energy coupling function and solar wind-magnetosphere dynamo. *Geophys Res Lett* **6(7)**: 577–580. https://doi.org/10.1029/gl006i007p00577.

Killeen TL, Won Y-I, Niciejewski RJ, Burns AG. 1995. Upper thermosphere winds and temperatures in the geomagnetic polar cap: Solar cycle, geomagnetic activity, and interplanetary magnetic field dependencies. *J Geophys Res Space Phys* **100(A11)**: 21327–21342. https://doi.org/10.1029/95ja01208.

Laundal KM, Cnossen I, Milan SE, Haaland SE, Coxon J, Pedatella NM, Förster M, Reistad JP. 2016. North–south asymmetries in earth's magnetic field: effects on high-latitude geospace. *Space Sci Rev* **206(1–4)**: 225–257. https://doi.org/10.1007/s11214-016-0273-0.

Lean JL, Meier RR, Picone JM, Emmert JT. 2011. Ionospheric total electron content: global and hemispheric climatology. *J Geophys Res Space Phys* **116(A10)**: A10318. https://doi.org/10.1029/2011JA016567.

Lei J, Thayer J, Forbes JM, Wu Q, She C, Wan W, Wang W. 2008a. Ionosphere response to solar wind high-speed streams. *Geophys Res Lett* **35**: L19105. https://doi.org/10.1029/2008GL035208.

Lei J, Thayer JP, Forbes JM, Sutton EK, Nerem RS. 2008b. Rotating solar coronal holes and periodic modulation of the upper atmosphere. *Geophys Res Lett* **35(10)**: L10109. https://doi.org/10.1029/2008gl033875.

Liou K, Newell PT, Meng C-I. 2001. Seasonal effects on auroral particle acceleration and precipitation. *J Geophys Res Space Phys* **106(A4)**: 5531–5542. https://doi.org/10.1029/1999ja000391.

Liou K, Wu C, Lepping RP, Newell PT, Meng C. 2002. Midday sub-auroral patches (MSPs) associated with interplanetary shocks. *Geophys Res Lett* **29(16)**: 1771. https://doi.org/10.1029/2001gl014182.

Liu H, Schlegel K, Ma S-Y. 2000. Combined ESR and EISCAT observations of the dayside polar cap and auroral oval during the May 15, 1997 storm. *Ann Geophys* **18(9)**: 1067–1072. https://doi.org/10.1007/s00585-000-1067-x.

Liu J, Liu L, Zhao B, Lei J, Thayer JP, McPherron RL. 2012. Superposed epoch analyses of thermospheric response to CIRs: solar cycle and seasonal dependencies. *J Geophys Res Space Phys* **117(A9)**: A00L10. https://doi.org/10.1029/2011ja017315.

Lockwood M, Cowley SWH, Freeman MP. 1990. The excitation of plasma convection in the high-latitude ionosphere. *J Geophys Res* **95(A6)**: 7961. https://doi.org/10.1029/ja095ia06p07961.

Lockwood M, Farmer A, Opgenoorth H, Crothers S. 1984. EISCAT observations of plasma convection and the high-latitude, winter F-region during substormactivity. *J Atmos Terr Phys* **46(6–7)**: 489–499. https://doi.org/10.1016/0021-9169(84)90067-9.

Lu G, Richmond AD, Lühr H, Paxton L. 2016. High-latitude energy input and its impact on the thermosphere. *J Geophys Res Space Phys* **121(7)**: 7108–7124. https://doi.org/10.1002/2015ja022294.

Ma SY, Cai HT, Liu HX, Schlegel K, Lu G. 2002. Positive storm effects in the dayside polar ionospheric F-region observed by EISCAT and ESR during the magnetic storm of 15 May 1997. *Ann Geophys* **20(9)**: 1377–1384. https://doi.org/10.5194/angeo-20-1377-2002.

Mendillo M. 2006. Storms in the ionosphere: Patterns and processes for total electron content. *Rev Geophys* **44(4)**: RG4001. https://doi.org/10.1029/2005RG000193.

Milan SE, Clausen LBN, Coxon JC, Carter JA, Walach M-T, et al. 2017. Overview of solar wind–magnetosphere–ionosphere–atmosphere coupling and the generation of magnetospheric currents. *Space Sci Rev* **206(1)**: 547–573. https://doi.org/10.1007/s11214-017-0333-0.

Miro G, de la Morena BA, Jakowski N. 1999. Equivalent slab thickness of the ionosphere in middle latitudes based on TEC/*foF2* observations over El Arenosillo. In: *COST 251/Workshop on Procedures and Testing of the Models for Ionospheric Telecommunications Application*, Hanbaba R, de la Morena Carretero BA (Eds.), Universidad de Huelva, Huelva, pp. 87–92. Available at http://digital.casalini.it/9788418984594.

Ogawa Y, Buchert SC, Sakurai A, Nozawa S, Fujii R. 2010. Solar activity dependence of ion upflow in the polar ionosphere observed with the European Incoherent Scatter (EISCAT) Tromsø UHF radar. *J Geophys Res Space Phys* **115(A7)**: A07310. https://doi.org/10.1029/2009ja014766.

Oyama S-i, Aikio A, Sakanoi T, Hosokawa K, Vanhamäki H, et al. 2023. Geomagnetic activity dependence and dawn-dusk asymmetry of thermospheric winds from 9-year measurements with a Fabry-Perot interferometer in Tromsø. *Norway. Earth Planet Space* **75(1)**: 70. https://doi.org/10.1186/s40623-023-01829-0.

Palmroth M. 2004. Role of solar wind dynamic pressure in driving ionospheric Joule heating. *J Geophys Res* **109(A11)**: A11302. https://doi.org/10.1029/2004ja010529.

Pedatella NM, Forbes JM. 2011. Electrodynamic response of the ionosphere to high-speed solar wind streams. *J Geophys Res Space Phys* **116(A12)**: A12310. https://doi.org/10.1029/2011ja017050.

Pedatella NM, Lei J, Thayer JP, Forbes JM. 2010. Ionosphere response to recurrent geomagnetic activity: local time dependency. *J Geophys Res Space Phys* **115(A2)**: A02301. https://doi.org/10.1029/2009JA014712.

Prölss G, Roemer M, Slowey J. 1988. Dissipation of solar wind energy in the Earth' supper atmosphere: the geomagnetic activity effect. *Adv Space Res* **8(5)**: 215–261. https://doi.org/10.1016/0273-1177(88)90043-9.

Rees MH, Emery BA, Roble RG, Stamnes K. 1983. Neutral and ion gas heating by auroral electron precipitation. *J Geophys Res Space Phys* **88(A8)**: 6289–6300. https://doi.org/10.1029/JA088iA08p06289.

Rentz S. 2009. The upper atmospheric fountain effect in the polar cusp region, *PhD Thesis*, Technical University Carolo-Wilhelmina zu Braunschweig. https://doi.org/10.2312/GFZ.B103-09050.

Ritter P, Lühr H, Maus S, Viljanen A. 2004. High-latitude ionospheric currents during very quiet times: their characteristics and predictability. *Ann Geophys* **22(6)**: 2001–2014. https://doi.org/10.5194/angeo-22-2001-2004.

Rodger AS, Wells GD, Moffett RJ, Bailey GJ. 2001. The variability of Joule heating, and its effects on the ionosphere and thermosphere. *Ann Geophys* **19(7)**: 773–781. https://doi.org/10.5194/angeo-19-773-2001.

Schunk R, Zhu L. 2008. Response of the ionosphere–thermosphere system to magnetospheric processes. *J Atmos Sol Terr Phys* **70(18)**: 2358–2373. https://doi.org/10.1016/j.jastp.2008.07.003.

Shirochkov A, Makarova L, Maurits S, Schlegel K. 1990. Response of the auroral ionosphere to solar wind parameter variations. *Ann Geophys* **8(5)**: 353–356.

Su Y-J, Caton RG, Horwitz JL, Richards PG. 1999. Systematic modeling of soft-electron precipitation effects on high-latitude F region and topside ionospheric upflows. *J Geophys Res Space Phys* **104(A1)**: 153–163. https://doi.org/10.1029/1998JA900068.

Tapping KF. 2013. The 10.7 cm solar radio flux (F10.7). *Space Weather* **11(7)**: 394–406. https://doi.org/10.1002/swe.20064.

Tesfaw HW, Virtanen II, Aikio AT. 2023. Characteristics of auroral electron precipitation at geomagnetic latitude 67 over Tromsø. *J Geophys Res Space Phys* **128(7)**: e2023JA031382. https://doi.org/10.1029/2023ja031382.

Thayer J, Lei J, Forbes J, Sutton E, Nerem R. 2008. Thermospheric density oscillations due to periodic solar wind highspeed streams. *J Geophys Res Space Phys* **113(6)**: A06307. https://doi.org/10.1029/2008JA013190.

Tsagouri I, Belehaki A. 2008. An upgrade of the solar-wind-driven empirical model for the middle latitude ionospheric storm-time response. *J Atmos Sol Terr Phys* **70(16)**: 2061–2076. https://doi.org/10.1016/j.jastp.2008.09.010.

Tsurutani B, Mannucci A, Iijima B, Abdu MA, Sobral JHA, et al. 2004. Global dayside ionospheric uplift and enhancement associated with interplanetary electric fields. *J Geophys Res Space Phys* **109(A8)**: A08302. https://doi.org/10.1029/2003JA010342.

Vaishnav R, Jacobi C, Berdermann J. 2019. Long-term trends in the ionospheric response to solar EUV variations. *Ann Geophys* **37**: 1141–1159. https://doi.org/10.5194/angeo-37-1141-2019.

Weimer DR. 2001. Maps of ionospheric field-aligned currents as a function of the interplanetary magnetic field derived from dynamics Explorer 2 data. *J Geophys Res Space Phys* **106(A7)**: 12889–12902. https://doi.org/10.1029/2000ja000295.

Wilson GR, Weimer DR, Wise JO, Marcos FA. 2006. Response of the thermosphere to Joule heating and particle precipitation. *J Geophys Res Space Phys* **111(A10)**: A10314. https://doi.org/10.1029/2005JA011274.

Workayehu AB, Vanhamäki H, Aikio AT. 2020. Seasonal effect on hemispheric asymmetry in ionospheric horizontal and field-aligned currents. *J Geophys Res Space Phys* **125(10)**: e2020JA028051. https://doi.org/10.1029/2020ja028051.

Zhang B, Lotko W, Brambles O, Wiltberger M, Wang W, Schmitt P, Lyon J. 2012. Enhancement of thermospheric mass density by soft electron precipitation. *Geophys Res Lett* **39(20)**: L20102. https://doi.org/10.1029/2012GL053519.

Zhang Q-H, Lockwood M, Foster JC, Zhang S-R, Zhang B-C, McCrea IW, Moen J, Lester M, Ruohoniemi JM. 2015. Direct observations of the full Dungey convection cycle in the polar ionosphere for southward interplanetary magnetic field conditions. *J Geophys Res Space Phys* **120(6)**: 4519–4530. https://doi.org/10.1002/2015ja021172.

Cite this article as: Borries C, Iochem P, Tasnim S & Davis F. 2024. Persistent high-latitude ionospheric response to solar wind forcing. *J. Space Weather Space Clim*. **14**, 33. https://doi.org/10.1051/swsc/2024029.